Submission	0 1 JUN. 2002
Revised	0 1 NOV. 2002
Accepted	1 7 DIC. 2002

Robust Flux and Speed Controller Design for Field Oriented Controlled Induction Motor Drives

N. Cumbria*, E.P. Nowicki*, A.H.M.A. Rahim**

*Dept of Electrical & Computer Engineering, University of Calgary,
Calgary, Alberta, Canada
**Dept of Electrical Engineering, King Fadh University of Petroleum and Minerals,
Dahran, Saudi Arabia

Abstract

The design of novel robust speed and rotor flux controllers for a field oriented controlled induction motor drive system is presented in this paper. The controllers are designed in terms of stability and performance criteria through a graphical technique, called loop-shaping, taking into account the effects of external disturbances and motor parameter deviations from the nominal model. Employing experimentally verified models, the controllers are tested using numerical simulations, for a large number of off-nominal parameter values. It is observed that for a doubling of the rotor resistance, the maximum absolute error in the flux magnitude is only 0.01 p.u. A comparison of the proposed controller approach with conventionally used proportional plus integral (PI) controllers indicates that PI controllers do not function in a stable manner even for an increase of 20% in rotor resistance.

Keywords

Robust control, induction motor drive, field oriented control.

1. Introduction

Induction motor drives have become the preferred choice in variable speed drive applications, in that an induction motor is superior in comparison to other electric machines with respect to structural simplicity, ease of maintenance, ruggedness, and durability. Compared with the DC motor in particular, the AC induction motor is better in terms of maximum speed capability, efficiency, size, weight and cost. However, the induction motor has proved inferior in terms of ease of control, due to its nonlinear and highly interacting multivariable control structure, whereas the separately excited DC motor's control structure allows for independent control of flux and torque.

In the late 1960's and early 1970's, Blaschke and Hasse [1-3] developed the principle of field oriented control (FOC), or vector control, for the purpose of high dynamic performance induction motor control. This technique permits the decoupling of flux and torque; thus allowing the induction motor to behave in a manner similar to a separately excited DC motor [4]. With FOC, it is possible to have the performance of a DC motor using a relatively low cost, simple, rugged squirrel cage induction motor.

The construction of the commercial induction motor does not allow the measurement of the rotor flux directly. However, with the assistance of a shaft speed sensor or speed estimator, the rotor flux magnitude and angular position can be estimated with one of several possible indirect field oriented control methods [5-9].

In indirect field orientation, the slip frequency is calculated using a speed input signal and time domain integration is performed to produce the slip angle and the rotor angle signals. These signals are then added to produce the instantaneous rotor flux position angle.

It is often desirable, in field oriented control applications, to keep the rotor flux magnitude at its rated value and that this condition should be obtained as quickly as possible upon start up. In some cases, it is possible to operate the motor above rated speed in a flux-weakening mode. Hence the usefulness of rotor flux control. Field oriented control also requires knowledge of rotor flux orientation so that current can be injected into the stator to obtain the commanded reference torque [4].

In past years, and still today, simple proportional plus integral (PI) controllers have been used in field orientation control schemes in industrial applications. As most high performance drives are subject to some types of external disturbances and parameter variations during normal operation, tuning and re-tuning of these controllers becomes a time consuming, yet necessary effort each time significant parameter variations occur. A need is established, then, for controllers that will provide good tracking and guaranteed performance levels despite any uncertainties present in the drive system. These uncertainties typically consist of differences in the dynamics of the model and the actual process, including various external load uncertainties, and plant parameter deviation, e.g. variation of the rotor time constant in an induction machine.

Robust control theory seems to provide an answer to this problem. In recent years, several advances have been made to reduce the hardware requirements of a field oriented control system [5, 10], and to improve the accuracy in speed and/or position control under a range of operating conditions through the use of robust control methods [6-9], thereby attempting to circumvent problems of plant uncertainties.

Following a graphical design method, called the loopshaping technique [11,12], it is proposed that a robust flux and a robust speed controller be developed in terms of high performance criteria, taking into account the effects of external disturbances and parameter variations, including changes in the inertia, as well as rotor and stator resistance alterations. In this paper, it is proposed that with the inclusion of robust controllers in the system modeling, changes in the values of the plant parameters may be compensated for.

2. Field Oriented Induction Motor Drive Model

Field oriented control implies that the stator current is oriented with respect to the rotor flux so as to attain independent control of flux and torque. The block diagram of an indirect field oriented induction motor drive is shown in Fig. 1 [13]. The robust controllers, the design of which will be given in the subsequent sections, are included in the flux and speed feedback loops. In order to achieve the desired currents for a system with a voltage source inverter, current controllers are needed to regulate stator voltages. PI controllers have been selected to do this.

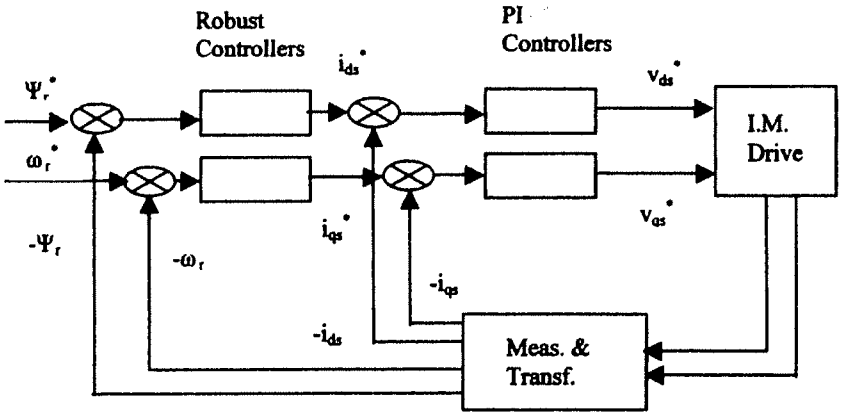

Fig. 1 Block diagram of induction motor drive system with indirect field oriented variables

The stator current supplied to the induction machine is divided into its direct (d) component, i_{ds}, and quadrature (q) component, i_{qs}, such that the time dependence of these quantities is removed for steady-state operation according to d-q axis theory [14,15]. The inputs to the system are the speed command (ω_r^*) and the flux command (Ψ_r^*). The d-q voltages are generated in the field oriented reference frame from the field oriented i_{ds} and i_{qs} feedback quantities. These voltages are then rotated, transformed and directly applied to a voltage source inverter. Field orientation results in

decoupled torque and rotor flux production, and therefore independent designs can be carried out for the controllers in the flux and speed loops.

Expressing the induction motor equations through field oriented variables along *d-q* axes, the dynamic current-flux and toque-speed equations can be expressed as [6,13],

$$\Psi_r = \frac{L_m}{sT_R + 1} i^*_{ds} \tag{1}$$

$$J\, d\omega_r/dt + B\omega_r = T_e - T_L = (p/2)L_m \tag{2}$$

where,

$$T_e = K_t\ i^*_{qs}\ ;\ \ K_t = (3p/4)(L_m^2/L_r)\, i^*_{ds} \tag{3}$$

Here, L_m is the magnetizing inductance, p is the number of poles, T_R is the rotor time constant L_r/R_r, L_r is rotor inductance, R_r is rotor resistance, T_e and T_L are electromechanical and load torques; J and B are the polar moment of inertia and coefficient of friction, respectively.

From equations (1)-(3), the following transfer functions $i^*_{ds} \rightarrow \Psi_r$ and $i^*_{qs} \rightarrow \omega_r$, for flux and speed control, respectively, are obtained.

$$\frac{\Psi_r}{i^*_{ds}} = P_f(s) = \frac{L_m}{sT_R + 1} \tag{4}$$

$$\frac{\omega_r}{i^*_{qs}} = P_s(s) = \frac{K_t}{Js + B} \tag{5}$$

Fig. 2 shows the simplified dynamic model of the induction motor.

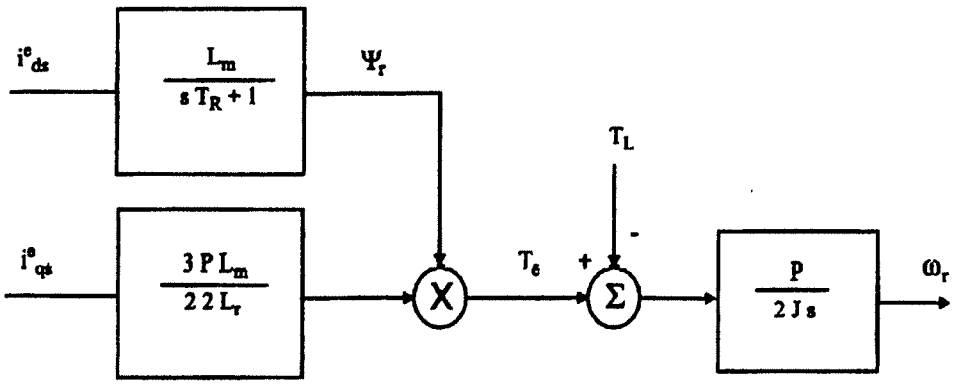

Fig.2 Dynamic model of the indirect FOC drive system

3. Uncertainty Modeling

Ideally, the performance of the control system should remain insensitive to the uncertainties of the drive system, which include differences in the dynamics of the model and the actual process,

such as external load disturbance, un-modeled and nonlinear dynamics of the plant, and plant parameter variations. The controllers should be 'robust' to perform satisfactorily under these varying conditions.

Unstructured uncertainty is one in which the modeling errors refer to the difference in the dynamics between the finite dimensional model and the unknown, and possibly infinite dimensional actual process [11]. In this article, the multiplicative representation of unstructured uncertainty is used to model the effects of plant parameter deviation and disturbance, defined in the Laplace domain as,

$$\tilde{P}(s) = [1 + \Delta(s) W_2(s)] P(s) \tag{6}$$

where, $\tilde{P}(s)$ is a perturbed plant transfer function, $\Delta(s)$ is a variable stable transfer function satisfying $\|\Delta(j\omega)\|_\infty \leq 1$, $W_2(s)$ is a fixed, stable, and proper transfer function also called the weight, which provides the uncertainty profile, $P(s)$ is the nominal plant (P_f or P_s for flux and speed, respectively) transfer function. The infinity norm (or ∞ - norm) of a function is defined here as the least upper bound of its absolute value,

$$\|\Delta(j\omega)\|_\infty = \sup_{\omega} |\Delta(j\omega)| \tag{7}$$

and is the highest gain value on a Bode magnitude plot.

There are several types of perturbations to be considered in system modeling. For both flux and speed control, one variable to be considered is the delay effect in system dynamics due to the coupling characteristics of the mechanical shaft, written as $e^{-\tau s}$, where τ is the dead-time of the drive, and $e^{-\tau s}$ is treated as a multiplicative uncertainty. A first order Pade approximation of $e^{-\tau s}$ is used to simplify the analysis [6, 11], where

$$e^{-\tau s} \approx \frac{1 - \tau s/2}{1 + \tau s/2} \tag{8}$$

The perturbed models in (6) take the form $\tilde{P}_f(s) \cdot e^{-\tau s}$ and $\tilde{P}_s(s) \cdot e^{-\tau s}$.

In the flux control loop, the rotor resistance, and hence T_R, is considered to be a perturbed variable due to temperature variations and skin effect during the normal operation of an induction motor. In the speed control system, the variables that are perturbed are the inertia, J, and the torque proportionality constant, K_t, which is a function of the flux command current, i_{ds}^*. This current, which is often set to a constant under FOC, is found to vary slightly during normal operation. The induction motor used in this drive system simulation is a 30HP, 415V, 2 poles, 50 Hz machine. Table 1 lists the nominal values of the parameters and their range of perturbations considered in this

study. A worst-case scenario has been considered by assuming the range of perturbations much higher than in actual motor performances.

TABLE 1: Parameters of the drive system

Parameters	Nom. value	Range
τ	0.025 *sec*	0.02 - 0.03
R_r	0.0287 p.u.	0.0287 – 0.04305
R_s	0.0147 p.u.	0.0147-0.02205
J	0.0167 p.u.	0.00835 - 0.0835
i_{ds}^{*}	0.3 p.u.	0.25 - 0.35

The motor parameters which are considered constant are: stator leakage reactance, $X_s = 0.1672$ p.u.; rotor leakage reactance, $X_r = 0.0916$ p.u; magnetizing reactance, $X_m = 3.1568$ p.u. It should be noted that this work does not take into consideration the effects of magnetic saturation.

Figs. 3(a) and 3(b) show the log-magnitude (L-m) plots of $\widetilde{P}_f$ and $\widetilde{P}_s$ for the range of parameters given in Table I, the bottom plot being for the smallest values of parameters. The L-m plots for the nominal plants are at the center. In (6), $\Delta(s)$ accounts for phase uncertainty and its magnitude varies between 0 and 1 at all frequencies. Hence, this term can be considered as a scaling factor on the magnitude of the perturbation.

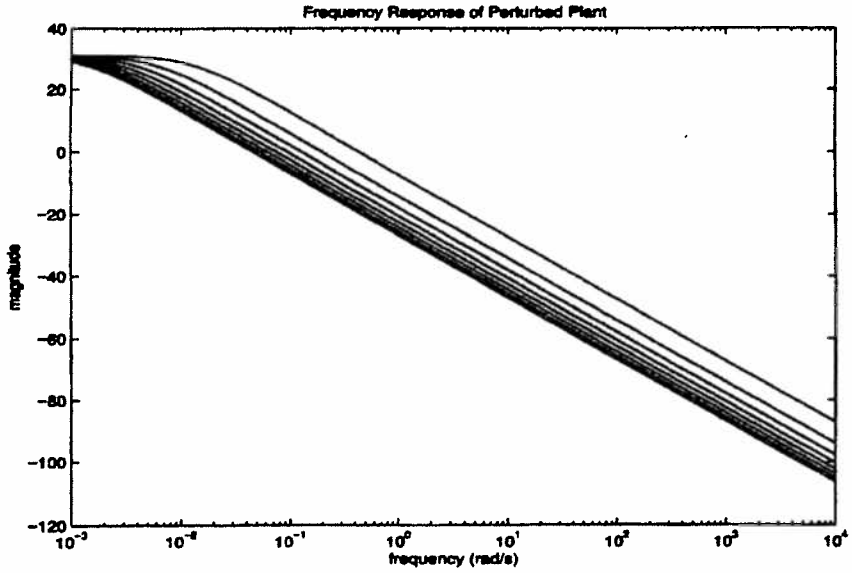

Fig. 3(a) The Log-magnitude plot for perturbed system for the ranges of parameters, Speed plant $\widetilde{P}_s$

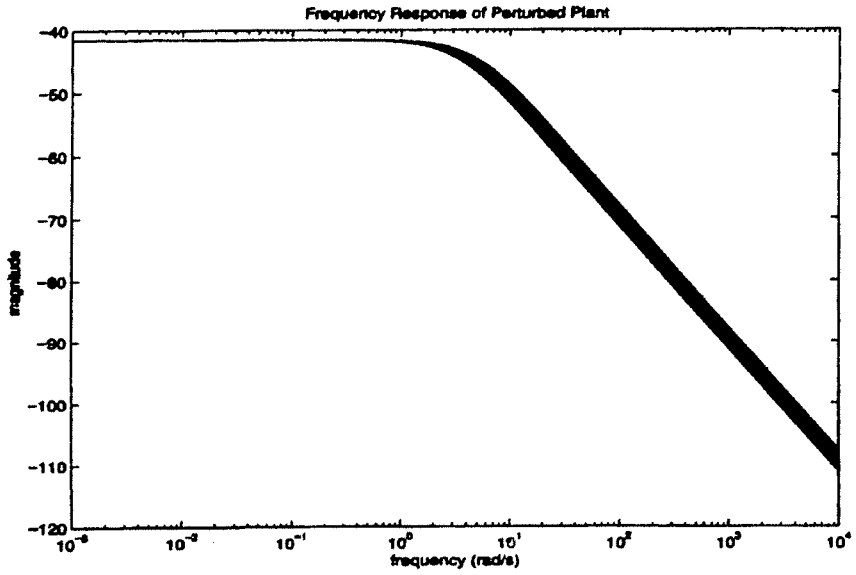

Fig. 3(b) The Log-magnitude plot for perturbed system for the ranges of parameters, the flux plant $\tilde{P}_f$

Interpreting the uncertainty model, it can be seen that $\Delta(s)W_2(s)$ is the normalized error in the transfer function of the perturbed system with respect to the nominal model, such that,

$$\frac{\tilde{P}(s)}{P(s)} - 1 = \Delta(s)W_2(s) \tag{9}$$

Hence, if $\|\Delta(j\omega)\|_\infty \leq 1$

$$\left|\frac{\tilde{P}(j\omega)}{P(j\omega)} - 1\right| \leq |W_2(j\omega)|\ , \text{ for all frequencies.} \tag{10}$$

This implies that $|W_2(j\omega)|$ provides the uncertainty profile. The L-m plots for the various W_2(s) functions are extracted from Figs. 3(a) and 3(b). The function W_2(s), which satisfies the asymptotic plot, is then constructed as

$$W_2(s) = \frac{0.04s}{0.01s + 1} \tag{11}$$

4. Robust Stability and Performance

A controller C(s) provides robust stability to the overall plant if it provides internal stability to each plant $\tilde{P}(s)$ with uncertainty. For the multiplicative perturbation model (6), the robust stability criterion is met iff [6,16],

$$\|W_2 T\|_\infty < 1 \tag{12}$$

where, T is the overall input-output transfer function given as,

$$T = \frac{PC}{1+PC} \tag{13}$$

Dependence on the Laplace variable s has been dropped for convenience. Further, nominal performance condition for the system is,

$$\|W_1 S\|_\infty < 1 \tag{14}$$

where, W_1 is a real, rational, stable, non-minimum phase transfer function, also called the weighting function. The sensitivity function S, defined to be the ratio between the error signal and the reference input, is,

$$S = 1 - T = \frac{1}{1+L} \tag{15}$$

Here, $L=PC$ is the open-loop transfer function. Using (7), the perturbed sensitivity function can be written as,

$$\tilde{S} = \frac{1}{1+\tilde{P}C} = \frac{S}{1+\Delta W_2 T} \tag{16}$$

A block diagram of a typical perturbed system ignoring all inputs is shown in Fig. 4(a), while a reduced configuration is given in Fig. 4(b).

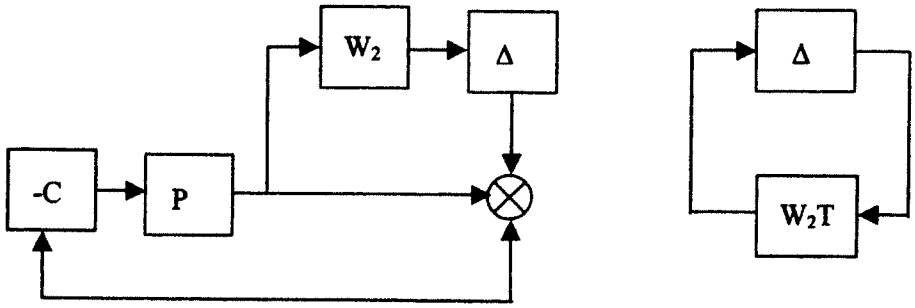

Fig.4 Perturbed feedback system, (a) original, (b) reduced

Since, $|\Delta| \le 1$, and,

$$\left\| \frac{W_1 S}{1+\Delta W_2 T} \right\|_\infty \le \left\| \frac{W_1 S}{1-|W_2 T|} \right\|_\infty < 1 \tag{17}$$

equations (12) and (14) can be combined to give the necessary and sufficient conditions for robust stability and performance of the control system as [9],

$$\| |W_1 S| + |W_2 T| \|_\infty < 1 \tag{18}$$

Equation (18) can then be shown to be equivalent to the condition,

$$\left| \frac{W_1}{1+L} \right| + \left| \frac{W_2 L}{1+L} \right| < 1, \text{ for all } \omega \tag{19}$$

5. Controller Design Through Loopshaping Technique

Loopshaping is a graphical design procedure for robust performance design, whereby P, W_1, and W_2 are the input data, and a proper controller C is designed to stabilize the plant and satisfy (19). Internal stability of the nominal feedback system and the properness of C constitute the constraints on this method. It is assumed that P and P^{-1} are both stable, otherwise L must contain unstable poles of P. Thus, the condition on L is that it must have no pole-zero cancellation.

A necessary condition for robust performance is that at every frequency, either $|W_1|$ or $|W_2|$ must be less than unity [11]. Typically, $|W_1|$ is monotonically decreasing for good tracking of low frequency signals, and $|W_2|$ is monotonically increasing as uncertainty increases with increasing frequency.

For low frequencies, we have $|W_1|>1>|W_2|$, implying

$$|L|>\frac{|W_1|}{1-|W_2|} \tag{20}$$

Similarly, since at high frequencies $|W_1|<1<|W_2|$, we have

$$|L|<\frac{1-|W_1|}{|W_2|} \tag{21}$$

From (20) and (21) we observe that for low frequencies $|L|>>1$, and for high frequencies $|L|<<1$.

For a choice of W_1 as a third order Butterworth filter given by,

$$W_1(s)=\frac{1.05}{s^3+2s^2+2s+1} \tag{22}$$

it is observed from simulation studies that a cut-off frequency of 1 *rad/s* provides good tracking over the normalized frequency range [0, 1] for both flux and speed control systems. At very high frequencies, $|L|$ should roll off at least as quickly as $|P|$ does. This ensures that the controller is proper. The general features of the open-loop transfer function, then, are that the gain in the low frequency region should be large enough, and in the high frequency region, the gain should be attenuated as much as possible. The gain at the intermediate frequencies typically controls the gain and phase margins. Near the gain crossover frequency ω_c, the transition from low to high frequency should be smooth. Therefore, it is desirable for the L-m plot to have a slope that is as close to –20 *dB/decade* as possible. If $|L|$ drops off too quickly through crossover, internal instability will result, so a gentle slope is crucial. For the selected W_1 and W_2 functions of equations (22) and (11) respectively, a stable, minimum-phase open-loop transfer function L is obtained as

$$L(s) = \frac{36(s+2)}{s(s^2+6s+9)} \tag{23}$$

The corresponding controllers for flux and speed, C_f and C_s, respectively, are recovered from the condition $L = PC$, and are given by

$$C_f = \frac{12.97s^2 + 61.94s + 72}{s(0.01s^2 + 0.00603s + 0.0904)} \tag{24}$$

$$C_s = \frac{0.6012s^2 + 1.206s + 0.0072}{s(0.0044s^2 + 0.0264s + 0.0395)} \tag{25}$$

The L-m plots for W_1, W_2 and L are shown in Fig. 5. The robust performance condition is verified by plotting $|W_1S| + |W_2T|$ in Fig. 6, where it can be seen that $\| |W_1S| + |W_2T| \|_\infty = 0.13 < 1$. On a trial and error basis, this is the best result that could be achieved with gain manipulation of L. The performance condition (14) is found to increase towards a magnitude of unity if the gain is manipulated either in the positive or negative direction.

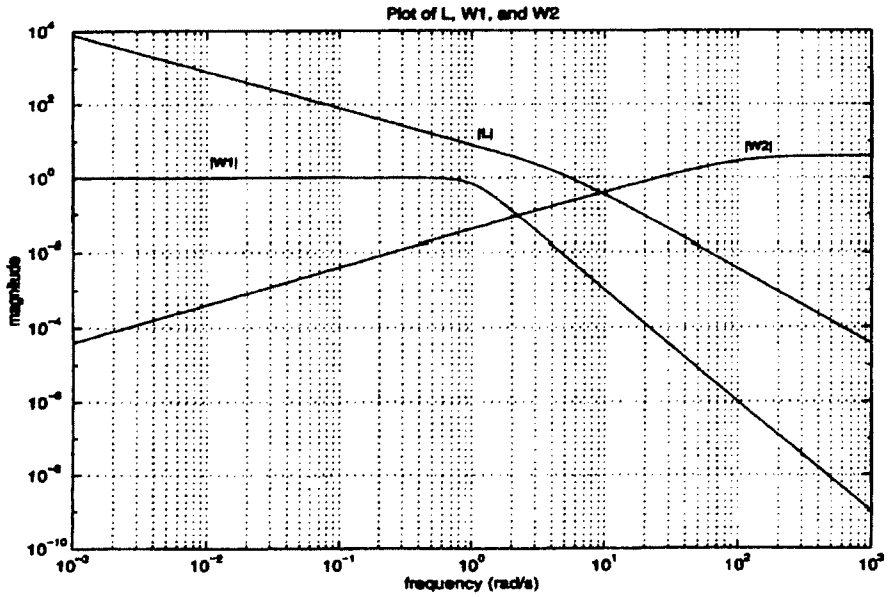

Fig.5 Log-magnitude plot of L, W_1 and W_2

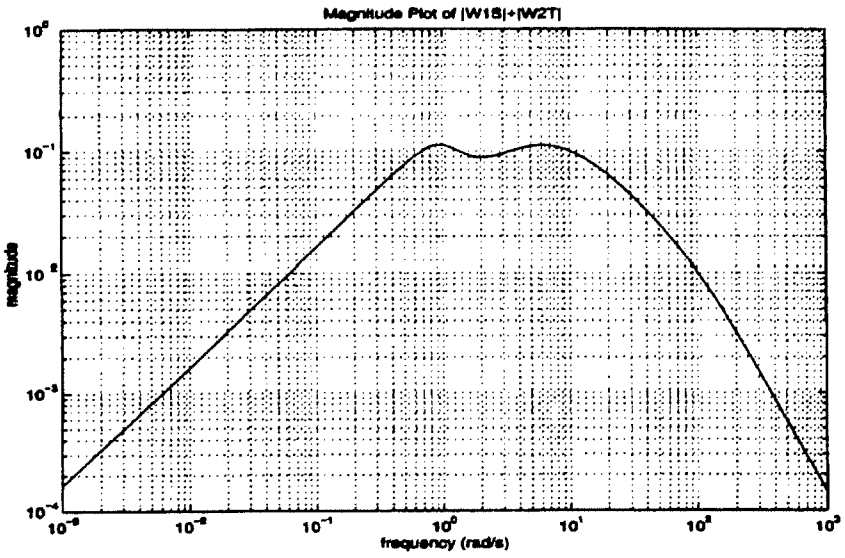

Fig. 6 Log-magnitude plot of $|W_1S|+|W_2T|$ for robust performance verification

The roots of the closed loop system $1 + L = 0$ are

$-2.0303 + j5.7448$ *rad/s*

$-2.0303 - j5.7448$ *rad/s*

-1.9394 *rad/s*

The damping ratio of the closed loop system is 0.33, verifying that L provides nominal internal stability.

6. Implementation and Results

The induction motor drive system shown in Fig. 1 is simulated to verify the robustness of the designed controllers. The dynamic model of the motor drive in field-oriented variables is coded in C language. The in-house developed *d-q* based induction motor model has been experimentally verified in previous knowledge-based induction motor control studies [17]. The robust controllers were designed using MATLAB, and then incorporated into the drive simulation by converting them from the continuous time domain of their MATLAB environment to the discrete time domain employed in the C program through bilinear transformation,

$$s = \frac{2}{T_s}\left(\frac{z-1}{z+1}\right) \tag{26}$$

The controllers are then converted to the discrete time domain in terms of difference equations in delay-operator form, defined by the controller input and output variables.

As shown in Fig. 1, the outputs of the robust controllers are the variables i_{ds}^* and i_{qs}^*. In order to achieve the desired currents for a system using a voltage source inverter, the current controllers are needed to regulate the stator voltages. These controllers are chosen to be PI controllers. In selecting the controller parameters, the proportional control coefficient is tuned first until the drive system just begins to become unstable. Then the integral coefficient is tuned to have the best steady-state error [13,16].

Figs. 7-9 show the variations of rotor speed, electromagnetic torque and flux magnitudes when the robust flux and speed controllers are implemented. The rotor speed shown in Fig. 7 is produced by toggling i_{qs}^* between 6.0 p.u. and –6.0 p.u. every 0.2 sec (i.e. the motor has a high stall torque rating). As can be seen from Fig. 9, the rotor flux magnitude reaches the value of 1.0 p.u. in less than 0.02 *sec* with the robust controllers implemented. This is a favorable result since our goal is for the rotor flux to reach its rated value as quickly as possible and maintain that magnitude throughout the normal operating range of the induction motor. Once the flux magnitude is set, current may be induced into the rotor at the point where the magnetic field strength is at its maximum.

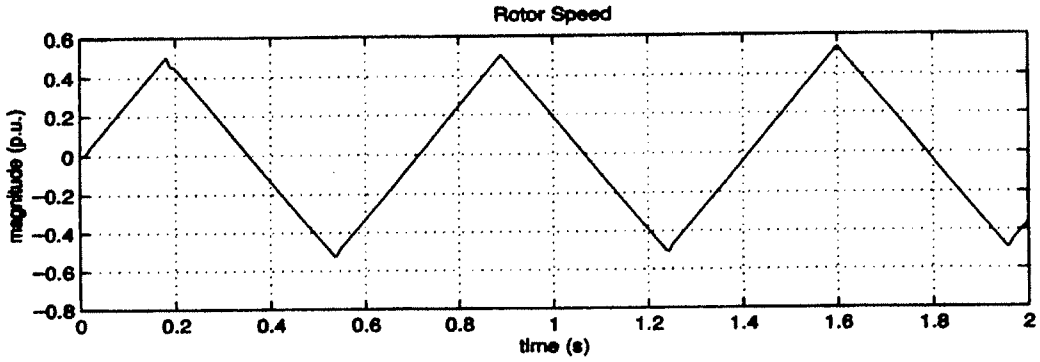

Fig. 7 Rotor speed of the induction motor with robust speed and flux controllers

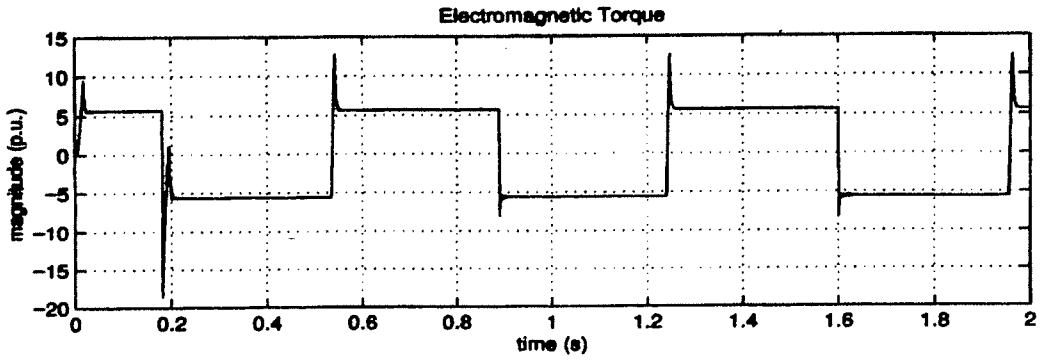

Fig. 8 The electromagnetic torque corresponding to Fig.7

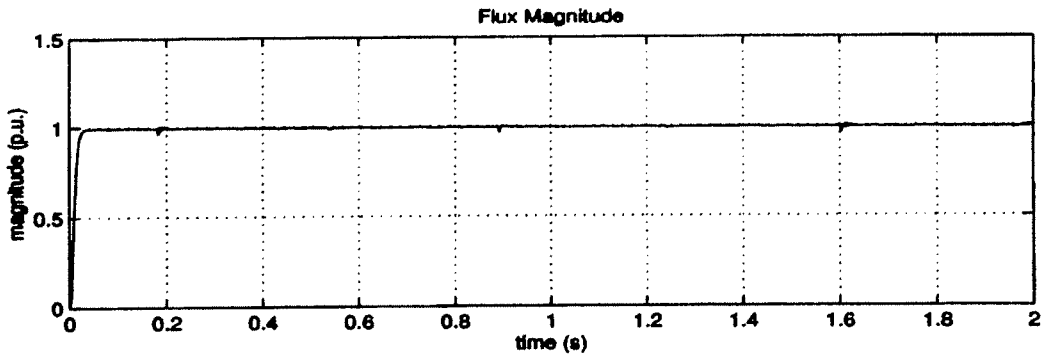

Fig. 9 The rotor flux magnitude corresponding to Fig.7

Since the robust controllers should remain insensitive to parameter variations, different types of uncertainties were included in the system modeling to test the effectiveness of the controllers. For the flux control system alone, the variation in rotor resistance, R_r, is the dominant factor affecting flux estimation in practice. To provide some indication of estimation sensitivity, the value of the rotor resistance is changed in the FOC program, without altering the robust controllers or any other parameters of the drive system.

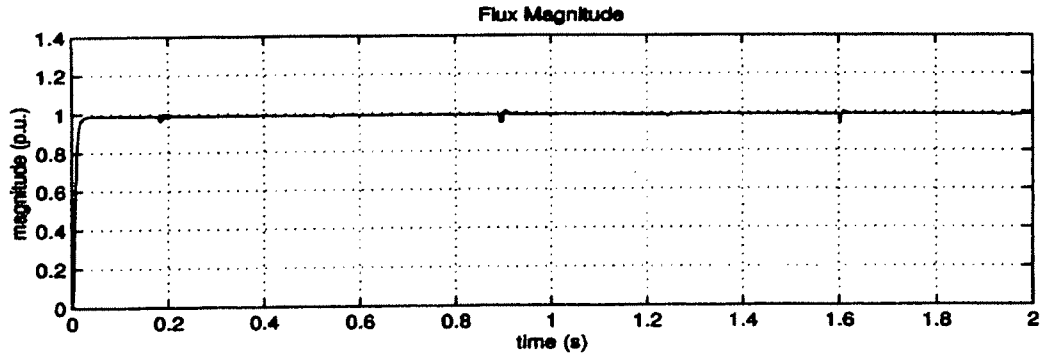

Fig. 10(a) Flux magnitude with the robust controllers, 50% increase in R_r

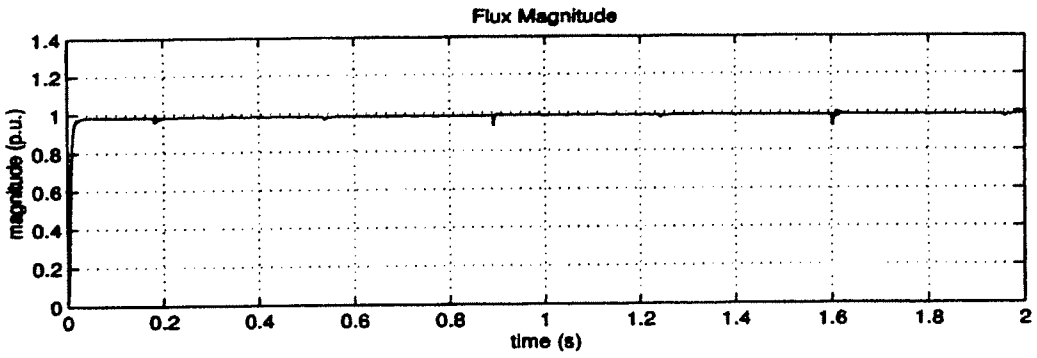

Fig. 10(b) Flux magnitude with the robust controllers, 100% increase in R_r

Fig. 10 shows a comparison of the flux magnitudes with the following two simulated values of the rotor resistance of the motor: (a) 50% increase in nominal value, and (b) with 100% increase.

Note that the robust controllers were designed for only a maximum variation of 50%. It can be seen that even for 100% variation in the resistance, the maximum absolute error is only 0.01 p.u. Fig. 11 gives a comparison of the flux magnitudes when the inertia constant J is varied. Plot (a) is for the case where J is increased to 5 times its nominal value, and (b) is for J decreased to 50%. As can be observed, the flux rises to rated value very fast. Expectedly, there are sharp spikes at the instants of toggling. Fig. 12 gives a comparison of the variations of the flux magnitude when the stator resistance is varied. Plot (a) is for a 20% increase from the nominal value, and (b) for a 50% increase. The fluxes reach the rated value almost at the same rate in the perturbed conditions, verifying the effectiveness of the robust controller.

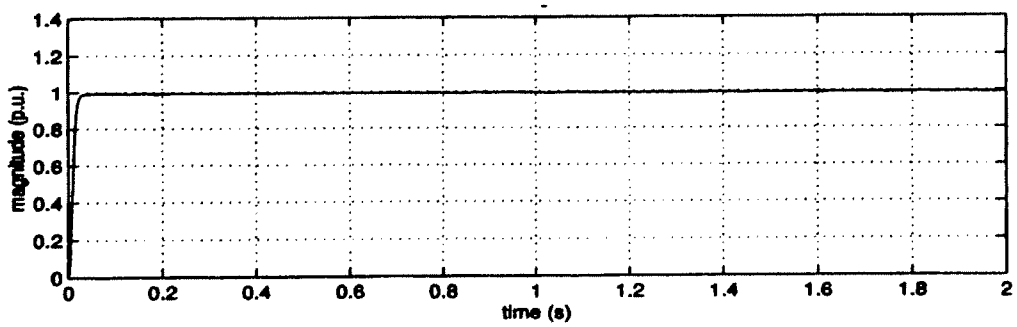

Fig. 11(a) Comparison of flux magnitude for different values of J, 5 times nominal value

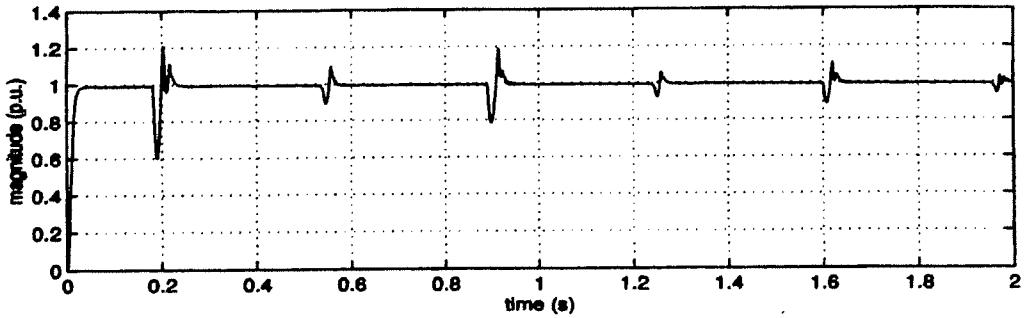

Fig. 11(b) Comparison of flux magnitude for different values of J, 50% less than nominal value

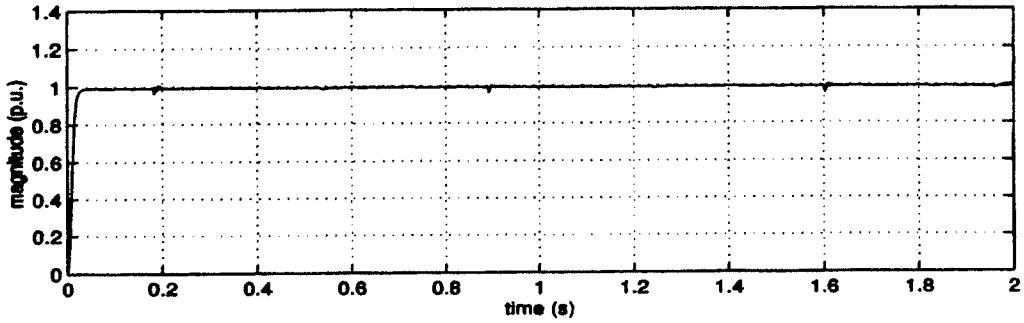

Fig. 12(a) Flux magnitude for different values of stator resistance, R_s increased by 20%

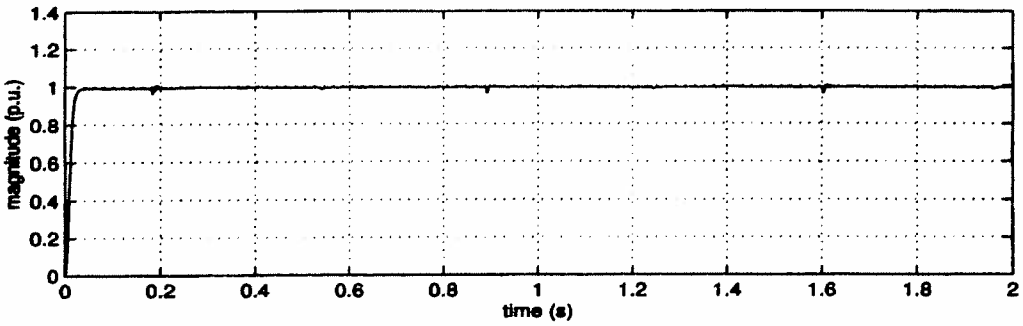

Fig. 12(b) Flux magnitude for different values of stator resistance, R_s increased by 50%

To further demonstrate the effectiveness of the robust controllers, their performance is compared with that of well-tuned PI controllers. PI control is still used to a great extent in industry due to the simplicity of its design and the ease of its implementation. Under nominal conditions where there is no parameter variation, the PI controllers provide results comparable to those of robust control, as shown in Figs. 8 and 9, which present torque and flux magnitude, respectively. It is observed that the flux magnitude reaches 1.0 p.u. in approximately 0.01 *sec*, which is slightly more favorable than the result achieved with robust control. However, it can be seen in Figs. 13 and 14 that with the same controller coefficients the PI controllers cannot regulate the flux magnitude if the rotor resistance increases more than 20% or inertial variations decreases less than 50% of the nominal setting.

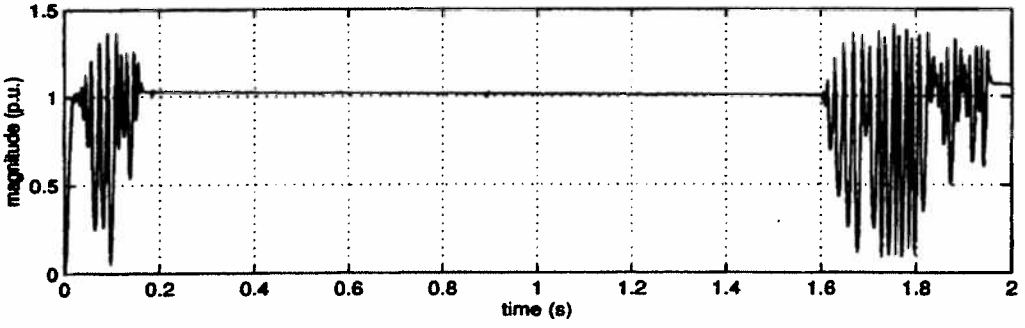

Fig. 13 Flux magnitude with PI controllers, R_r increased by 20%

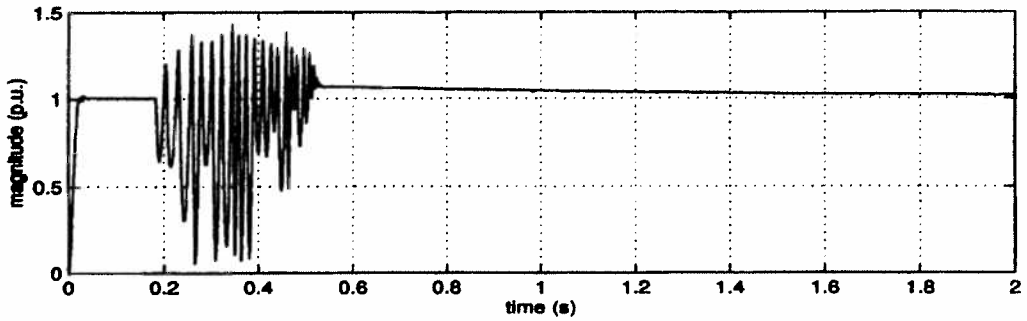

Fig. 14 Flux magnitude with PI controllers, J decreased by 50%

7. Conclusions

Novel robust flux and speed controllers for an indirect FOC induction motor drive are presented in this article. The controllers are designed for robust stability and performance using the loopshaping technique. It has been observed that with the robust controller, the flux magnitude reaches its rated value of 1.0 p.u. quickly, in under 0.02 *sec*, and maintains that value throughout the operating range of the motor. The system's ability to accurately estimate the rotor flux despite parameter variations is verified by test cases and comparisons. Though the robust controller is designed for a 50% variation of rotor resistance, it is observed that the maximum absolute error is only 0.01 p.u. for a 100% increase in rotor resistance. In practice, rotor resistance varies about 20%, arising primarily from temperature variation. Hence the small sensitivity to rotor resistance variation of the proposed robust controller, suggests nominal operation can be achieved in practice over a wider range of parameter variation than in the case of the industry standard PI controller. Further studies are planned that will incorporate nonlinear effects, such as magnetic saturation.

Employing an experimentally tested induction motor model, the effectiveness of the robust controllers has been verified through simulation studies, by considering significant variations in rotor and stator resistances and the inertia parameter. The design procedure for the robust controller is simple and straightforward.

References

1. F. Blaschke, "Das Verfahren der Feldorientierung zur Regelung der Asynchronmaschine," Siemens Forsch. –u. Entwickl. –Ber. Vol.1, no. 1, pp. 184 – 193, 1972.
2. F. Blaschke, "The principle of field orientation as applied to the new TRANSVECTOR closed loop control system for rotating field machines," Siemens Review, Vol. 34, pp. 217 – 220, May 1972.

3. K. Hasse, " On the dynamic behavior of induction machines driven by variable frequency and voltage sources," ETZ – A Bd 89 H. 4, pp. 77 – 81, 1968.
4. R. Jonsson, "Natural Field Orientation (NFO) Provides Sensorless Control of AC Induction Servo Motors," PCIM, pp. 44 – 51, June 1995.
5. A. Hughes, J. Corda, D. A. Andrade, "Vector Control of cage induction motors: a physical insight," IEE Proc. -Elect. Power App., Vol. 143, no. 1, pp. 59 – 68, January 1996.
6. G. M. Liaw, F. J. Lin, "A Robust Speed Controller for Induction Motor Drives," IEEE Transactions on Industrial Electronics, Vol. 41, No. 3, pp. 308 - 315, June 1994.
7. Y. Y. Tzou, "DSP-Based Robust Control of an AC Induction Servo Drive for Motion Control," IEEE Transactions on Control System Technology, Vol. 4, No. 6, pp. 614 - 626, November 1996.
8. F. J. Lin, "Robust speed-controlled induction motor drive using EKF and RLS estimators," IEE Proc. -Elect. Power App., Vol. 143, no. 3, pp. 186 - 192, May 1996.
9. D. R. Chouiter, G. Clerc, P. Auriol, J. M. Retif, "On the robust control of an induction machine: a complete design and realization," EPJ Applied Physics, V. 6 no1, pp. 61 – 70,1999.
10. H. Kim, M. Shin, D. Hyun, "Improved Vector Control of an Induction Motor with On-Line Tuning of Its Parameters," IECON 98 Proceedings of the 24th Annual Conference of the IEEE Industrial Electronics Society, pp. 854 – 858, August 1998.
11. W. S. Levine, *The Control Handbook*, CRC Press & IEEE Press, 1996.
12. M. Green, D. J. N. Limebeer, *Linear Robust Control*, Prentice Hall, 1995.
13. A. K. P. Toh, E. P. Nowicki, F. Ashrafzadeh, "A Flux Estimator for Field Oriented Control of an Induction Motor Drive," IEEE IAS Annual. Meeting Conf. Record, pp. 585 – 592, October 1994.
14. P. C. Krause, *Analysis of Electric Machinery*, McGraw-Hill, 1986, pp. 133 - 179.
15. B. K. Bose, *Power Electronics and Variable Frequency Drives*, IEEE Press, 1997.
16. J. R. Smith, A.J. Tait, "Electrical drive simulator for teaching purposes," IEE Proceedings, Vol. 135, Pt. A, no. 1, pp. 29-32, January 1998.
17. M. Mohamadian, E. P. Nowicki, F. Ashrafazdeh, R. Sachdeva, A. Chu, E. Evanik, "A Novel Neural Network Controller and Its Efficient DSP Implementation for Vector Controlled Induction Motor Drives," IEEE IAS Annual Meeting, pp. 1455 – 1462, October 2002.